NeuroImage 53 (2010) 1023–1029

Contents lists available at ScienceDirect

NeuroImage

journal homepage: www.elsevier.com/locate/ynimg

Anatomical phenotyping in a mouse model of fragile X syndrome with magnetic resonance imaging

Jacob Ellegood [a,*], Laura K. Pacey [b], David R. Hampson [b], Jason P. Lerch [a], R. Mark Henkelman [a]

[a] Mouse Imaging Centre, The Hospital for Sick Children, Toronto, Ontario, Canada
[b] Leslie Dan Faculty of Pharmacy, University of Toronto, Toronto, Ontario, Canada

ARTICLE INFO

Article history:
Received 2 September 2009
Revised 11 March 2010
Accepted 12 March 2010
Available online 19 March 2010

Keywords:
fragile X syndrome
magnetic resonance imaging
deep cerebellar nuclei
immunohistochemistry

ABSTRACT

Fragile X Syndrome (FXS) is the most common single gene cause of inherited mental impairment, and cognitive deficits can range from simple learning disabilities to mental retardation. Human FXS is caused by a loss of the Fragile X Mental Retardation Protein (FMRP). The fragile X knockout (FX KO) mouse also shows a loss of FMRP, as well as many of the physical and behavioural characteristics of human FXS. This work aims to characterize the anatomical changes between the FX KO and a corresponding wild type mouse. Significant volume decreases were found in two regions within the deep cerebellar nuclei, namely the nucleus interpositus and the fastigial nucleus, which may be caused by a loss of neurons as indicated by histological analysis. Well-known links between these nuclei and previously established behavioural and physical characteristics of FXS are discussed. The loss of FMRP has a significant effect on these two nuclei, and future studies of FXS should evaluate the biochemical, physiological, and behavioral consequences of alterations in these key nuclei.

Introduction

The most common inherited form of mental retardation, Fragile X Syndrome (FXS), affects approximately 1 in 4000 males and 1 in 8000 females (Crawford et al., 2001; Visootsak et al., 2005). FXS results from a trinucleotide repeat expansion mutation in the X-linked Fragile X Mental Retardation 1 (FMR1) gene. Methylation of the FMR1 promoter causes gene silencing and loss of expression of the protein product, fragile X mental retardation protein (FMRP). Individuals with FXS exhibit a range of symptoms, including mild to moderate mental retardation, anxiety, hyperactivity, autistic-like behaviours and seizures (O'Donnell and Warren, 2002). Common physical characteristics include a long narrow face, large protruding ears and enlarged testicles (Visootsak et al., 2005).

The FMR1 knockout mouse (FX KO), first created in 1994 (Dutch-Belgium Fragile X Consortium, 1994), is the most common animal model used to study FXS. The FX KO does not express FMRP and displays many characteristics associated with FXS in humans including learning deficits, hyperactivity, seizures and enlarged testicles (Musumeci et al., 2000; Oostra and Hoogeveen, 1997; Pacey et al., 2009). Both humans and mice also exhibit an abundance of long, thin immature dendritic spines in the cerebral cortex, hippocampus and cerebellum, suggesting abnormal synaptic development and/or maturation in the absence of FMRP (Grossman et al., 2006; Irwin et al., 2000; Koekkoek et al., 2005). The first brain abnormality reported in a Magnetic Resonance Imaging (MRI) study of human FXS carriers was underdevelopment of the cerebellar vermis (the tissue connecting the right and left hemisphere of the cerebellum) (Reiss et al., 1988). Abnormalities in the development of the cerebellar vermis have been mentioned in a large number of studies, and are thought to be directly related to some of the behavioural deficits in fragile X syndrome, since the vermis has connections to the amygdala and hippocampus (Hessl et al., 2004). Other MRI studies have shown abnormalities in the fourth ventricle (Mostofsky et al., 1998; Reiss et al., 1991), the hippocampus (Reiss et al., 1994), and the amygdala (Reiss et al., 1995). Diffusion Tensor Imaging (DTI) has also found lower Fractional Anisotropy (FA) values in fronto-striatal pathways and in parietal sensory motor tracts (Barnea-Goraly et al., 2003) indicating a loss of order/structure in those pathways.

A previous MRI study on the FX KO mouse did not find any volume changes in the brain (Kooy et al., 1999); however, the analysis was performed on very large brain structures and the resolution was quite low. The purpose of this paper was to determine if there are any detectable anatomical and/or white matter structural changes in the FX KO mouse model when compared to the wild type (WT) mice using high-resolution MRI and DTI. Furthermore, we assess changes to the craniofacial structure with high-resolution micro-CT in order to look for skeletal changes due to the known facial dismorphism associated with human FXS.

* Corresponding author. Mouse Imaging Centre (MICe), Hospital for Sick Children, Toronto Centre for Phenogenomics, 25 Orde Street, Toronto, Ontario, Canada M5T 3H7. Fax: +1 647 837 5832.
E-mail address: jacob@phenogenomics.ca (J. Ellegood).

1053-8119/$ – see front matter © 2010 Elsevier Inc. All rights reserved.
doi:10.1016/j.neuroimage.2010.03.038

Materials and methods

Specimen preparation

Fourteen, fixed C57BL6 mouse brains left in the skull (7 FX KO mice and 7 WT mice) were examined at age P30 (postnatal day 30). P30 was chosen because this is the age where the FX KO mice were the most susceptible to the audiogenic seizures associated with the mouse model (Musumeci et al., 2000; Pacey et al., 2009). Initially the mice were anesthetized with ketamine/xylazine and intracardially perfused with 30 mL of 0.1 M PBS containing 10 U/mL heparin (Sigma) and 2 mM ProHance (a Gadolinium contrast agent) followed by 30 mL of ice cold 4% paraformaldehyde (PFA) containing 2 mM ProHance (Spring et al., 2007). Perfusions were performed with a Pharmacia minipump at a rate of approximately 100 mL/h. After perfusion, mice were decapitated and the skin, lower jaw, ears, and the cartilaginous nose tip were removed. The brain and remaining skull structures were incubated in 4% PFA + 2 mM ProHance overnight at 4 °C then transferred to 0.1 M PBS containing 2 mM ProHance and 0.02% sodium azide for at least 7 days prior to MRI scanning.

Magnetic resonance imaging

A 7.0 Tesla MRI scanner (Varian Inc., Palo Alto, CA) with a 6-cm inner bore diameter insert gradient (max gradient 100 G/cm) was used for all MRI scans. Three custom built solenoid coils were used to image three brains in parallel (Bock et al., 2005). Parameters used for anatomical MRI scans were optimized for high efficiency and gray/white matter contrast: T2-weighted, 3D fast spin echo, with a TR of 325 ms, and TEs of 10 ms per echo for 6 echoes, with the centre of *k*-space being acquired on the 4th echo, four averages, field-of-view of $14\times14\times25$ mm^3 and matrix size of $432\times432\times780$ giving an image with 0.032 mm isotropic voxels. Total imaging time for this MRI sequence is ~12 h (Henkelman et al., 2006).

DTI scanning was performed with a 3D diffusion-weighted fast spin echo sequence. Parameters used in the DTI sequence: echo train length of 6, TR of 325 ms, first TE 30 ms and a TE of 6 ms for the remaining 5 echoes, ten averages, field-of-view of $14\times14\times25$ mm^3 and a matrix size of $120\times120\times214$ yielding an image with 0.117 mm isotropic voxels. One $b=0$ image (with minimal diffusion weighting) and 6 high *b*-value images ($b=1956$ s/mm^2) were acquired in six different directions [(1, 1, 0),(1, 0, 1),(0, 1, 1),(−1, 1, 0),(−1, 0, 1),(0, 1, −1)] of (G_x, G_y, G_z). Total imaging time for this sequence was ~16 h. Fractional Anisotropy (FA) maps were then calculated (Le Bihan et al., 2001).

Computed tomography

After the MRI scans were completed the fixed mouse brains in skulls were scanned for craniofacial abnormalities. Three-dimensional CT images were acquired using a MS-9 micro-CT scanner (GE Medical Systems, London, Ontario, Canada) with the X-ray source set at 80 kVp. Craniofacial images were acquired in ~3 h with 720 views and reconstructed on a 0.02-mm isotropic grid. The computed images show calcified bone as highly intense against a relatively uniform dark background.

Registration and analysis

To visualize and compare any changes in the FX KO mouse, the brains (from the anatomical scan as well as the $b=0$ images from the DTI scans) and the skulls from the CT are linearly (6 parameters followed by 12 parameters) and nonlinearly registered towards a pre-existing atlas (Dorr et al., 2008) for the MRI scans and a wild type skull for the CT scans, and a transform is created for each mouse. All scans are then resampled with the appropriate transform and averaged to create a population atlas representing the average anatomy or skeletal structure of the study sample. All registrations are performed using the mni_autoreg tools (Collins et al., 1994). The result of the registration is to have all scans deformed into exact alignment with each other in an unbiased fashion. This allows for the analysis of the deformations needed to take each individual mouse's anatomy into this final atlas space, the goal being to model how the deformation fields relate to genotype (Lerch et al., 2008; Nieman et al., 2006). The determinants of the deformation fields were then calculated as measures of volume at each voxel. Significant volume and shape changes can then be calculated by warping a pre-existing classified MRI atlas onto the population atlas (Dorr et al., 2008), which allows the volume of 62 segmented structures encompassing cortical lobes, large white matter structures (i.e. corpus callosum), ventricles, cerebellum, brain stem, and olfactory bulbs (Dorr et al., 2008) to be assessed in all 14 brains. Since the mice at P30 are still developing, the 62 volumes were calculated as a percentage of total brain volume; furthermore, the voxel-wise analyses were also corrected for total brain volume. For the DTI data set, the transformations applied to the $b=0$ images during the registration process were applied to the calculated FA map for each brain, from which average FA maps were calculated for both the FX KO and the WT mouse. The intensities (i.e. the FA values) of the FA maps were then compared. FA differences were assessed on a voxel by voxel basis constrained by the white matter structures in the classified atlas (Dorr et al., 2008), and by measuring the mean FA values of the same white matter regions assessed in the anatomical MRI measurements. Multiple comparisons were controlled for using the False Discovery Rate (FDR) (Genovese et al., 2002).

Immunohistochemistry

The 14 fixed mouse brains were removed from the skull and paraffin embedded. 32 consecutive coronal slices (thickness 5 μm) were taken from each of the 14 mice through the cerebellum which included contributions from the dentate nucleus, fastigial nucleus, and nucleus interpositus. The vestibulocerebellar nucleus was not quantified. 8 slices each were stained with the following four antibodies: rabbit anti-Glial Fibrillary Acidic Protein (GFAP, 1:100, SIGNET), mouse anti-Neuronal Nuclei (NeuN, 1:100, Chemicon), rabbit anti-Vesicular GABA Transporter (VGAT, 1:1000, Synaptic Systems), and mouse anti-Vesicular Glutamate Transporter 1 (VGLUT1, 1:500, MediMabs). The slides were digitized by using a slide scanner at 40× resolution for each of the 4 stains. The dentate nucleus, fastigial nucleus, and nucleus interpositus were manually outlined (blinded to genotype) on the 32 sections per brain (Fig. 1A). A neural net classifier (Zijdenbos et al., 2002) was then trained to discriminate between active stain (GFAP, NeuN, VGAT, or VGLUT), counter stain (DAPI), and background (Fig. 1B, C). The same classification rules were applied to each and every slide of the same stain. The proportion of pixels stained by the active stain was then measured within each of the nuclei and used for subsequent quantitative analyses.

Results

The first step in our analysis was to examine the volume of the 62 different anatomical regions in the mouse brain using MRI (Dorr et al., 2008), as well as the total brain volume. Of the 62 segmented regions, one yielded significance: the arbor vita of the cerebellum, which is composed of the white matter in the cerebellum as well as the deep cerebellar nuclei; trends were found in the striatum, and the cerebral cortex of the parieto-temporal lobe. Table 1 lists the volume measurements (in % total brain volume) for the FX KO and WT mouse. The arbor vita of the cerebellum and the striatum both decreased in size in the FX KO mice, whereas the cerebral cortex of the

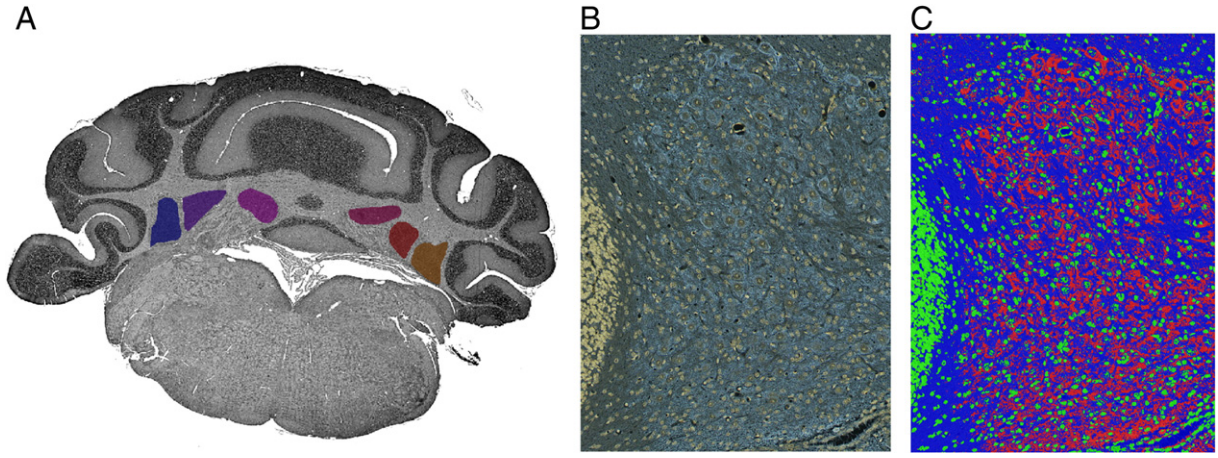

Fig. 1. Histological methodology. (A) The manual outlining of the specific nuclei. (B) A high-resolution image of the dentate nucleus in a WT mouse showing the active stain in blue (in this case VGAT), counter stain in yellow, and background in gray. (C) Same image as in B after classification.

parieto-temporal lobe increased when compared to the WT mice. The arbor vita of the cerebellum was a highly significant change with a q value of 0.02.

The significance of the volume change in the arbor vita led us to examine the cerebellum on a voxel by voxel basis in order to determine where the changes were located. Fig. 2A highlights the areas demonstrating significant decreases in FX KO mice, with the t-statistic in colour thresholded to a FDR of <10%. Fig. 2B shows a 3D representation of those significant areas in the cerebellum and shows specific localized volume changes that seem to be located within the deep cerebellar nuclei in the arbor vita. Based on these results, the dentate nucleus, the fastigial nucleus, the nucleus interpositus, and the vestibulocerebellar nucleus were hand segmented onto the registered anatomical average (Fig. 3), and the volumes of those 4 nuclei (total volume included the left and the right nuclei for each) were calculated for each brain after first resampling the cerebellar segmentation to each individual scan using the non-linear transforms created earlier. Fig. 3 plots the volumes of the individual cerebellar nuclei (in % total brain volume) for both the FX KO and WT mouse and shows the location of the 4 nuclei. Significant decreases in the volumes of the fastigial nucleus ($q=0.07$) and nucleus interpositus ($q=0.02$) were found in the FX KO mice compared to WT.

DTI revealed no significant changes in the white matter structures of the FX KO compared to the WT mouse. Furthermore, the craniofacial images which were acquired using the micro-CT also did not reveal any statistically significant skeletal deformities.

Immunohistochemistry

Since the MRI results indicated specific volumetric changes in the fastigial nucleus and nucleus interpositus, histology was performed on these regions, plus the dentate nucleus, in order to interpret these volumetric changes. The same 14 brains were analyzed by immunohistochemistry and stained for the astrocyte marker GFAP, the neuronal marker NeuN, the glutamate transporter VGLUT1 and the GABA transporter VGAT. GFAP and NeuN were chosen to determine the contributions of astrocytes and neurons within the cerebellar nuclei. VGAT and VGLUT1 were chosen because of previously reported increases in inhibitory synaptic transmission that have been shown in mouse models of autism (Tabuchi et al., 2007).

The histological data were analyzed by first looking for correlations between the proportions of active stain within the individually segmented cerebellar nuclei versus the corresponding volume changes in those cerebellar nuclei assessed by MRI (Fig. 4). A linear model of the normalized MRI volumes of the cerebellar nuclei versus the proportion stained of each of the 4 stains within each of those individual cerebellar nuclei revealed that ~50% ($R^2=0.454$, with $p=0.00115$) of the variance in the MRI volumes can be explained by the histology performed. Fig. 5 shows the differences in proportion stained in each of the three regions for each of the 4 histological stains performed between the WT and FX KO. A significant increase in the proportion of GFAP staining ($q<0.01$) and a significant decrease in the proportion of NeuN staining ($q<0.01$) was found in the examined deep cerebellar nuclei in the FX KO mouse compared with the WT. No significant changes in the proportion stained by VGAT and VGLUT1 were found between genotype.

Table 1
Volume measurements[a] for significantly different or trending regions in the fragile X knockout mouse and the wild type control mouse.

Region	Fragile X knockout	Wild type	p-value	q-value
Arbor vita of the cerebellum	1.98 ± 0.03	2.04 ± 0.03	0.0002	0.02
Parieto-temporal lobe	17.78 ± 0.26	17.36 ± 0.33	0.0077	0.16
Striatum	4.48 ± 0.12	4.56 ± 0.09	0.0076	0.16

[a] Volume measurements are listed in % total brain volume.

Discussion

The volume differences found in the deep cerebellar nuclei of FX KO mice are the most intriguing finding in this study. It would seem that the loss of volume, reported from the MRI measurements, in the fastigial nucleus and the nucleus interpositus may be related to the decrease in the proportion of neurons within the nuclei found in the histology. These findings suggest that the absence of FMRP results in a loss of neurons in the deep cerebellar nuclei. FMRP is highly expressed in the cerebellum (Nimchinsky et al., 2001) and it is unclear whether the neuronal loss seen in our study is a product of the absence of FMRP in deep cerebellar nuclei neurons or results from changes in surrounding cells, such as Purkinje cells, which exhibit altered spine morphology in the absence of FMRP (Koekkoek et al., 2005). In addition, recent evidence suggests the loss of FMRP may result in excess excitatory signaling in a number of brain regions (Curia et al., 2009; Gruss and Braun, 2001, 2004; Pacey et al., 2009). This could lead to excitotoxicity and neuronal loss in the deep cerebellar nuclei. Further studies are needed to determine the mechanism by which the loss of FMRP results in volume changes in the deep cerebellar nuclei.

Histological analysis also noted an increase in the proportion of GFAP staining in the cerebellar nuclei indicating an increase in the proportion of astrocytes in these regions. This increase could result from reactive gliosis in response to the neuronal loss. However, FMRP

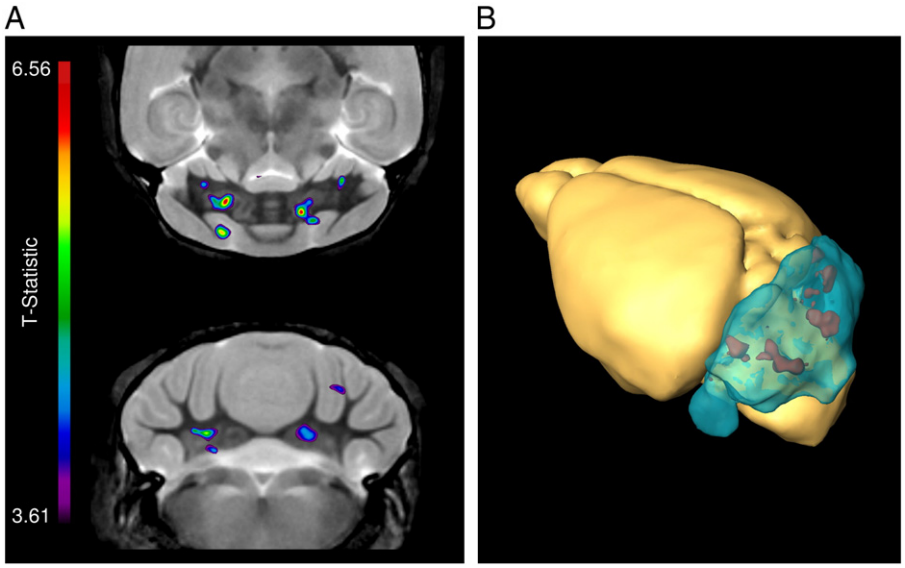

Fig. 2. (A) Significant volume decreases are highlighted (represented by their *t*-statistic) in the cerebellum of the fragile X knockout mouse when compared to the wild type. (B) 3D representation of the significant regions (red) in the cerebellum (blue). The regions highlighted in both A and B have a false discovery rate of <10%. This figure has been smoothed by tri-linear interpolation.

has also been recently shown to be expressed in astrocytes during development (Pacey and Doering, 2007) and loss of astrocytic FMRP affects neuronal morphology and dendritic branching in co-culture experiments (Jacobs and Doering, 2009). These findings suggest that the absence of FMRP in both neurons and astrocytes could contribute to the anatomical changes observed in the cerebellum.

Morphological and functional changes have been described previously in cells of the cerebellum in FX KO mice. A recent paper by Koekkoek et al. (2005) demonstrated immature dendritic spines in the Purkinje cells in the cerebellum of FX KO mice. That paper also noted a learning deficit in eye-blink conditioning in both FMR1 knockout mice and Purkinje cell-specific FMR1 knockouts. The eye-blink paradigm is controlled largely by structures such as the interpositus nucleus (Freeman and Nicholson, 2000; Thompson and Steinmetz, 2009). This learning deficit may, therefore, be a correlate of the volume changes and corresponding neuronal loss found in this study in the FX KO mouse.

Much of the attention on cerebellum changes in the human FXS as well as in autism spectrum disorders (ASDs) has been on changes in

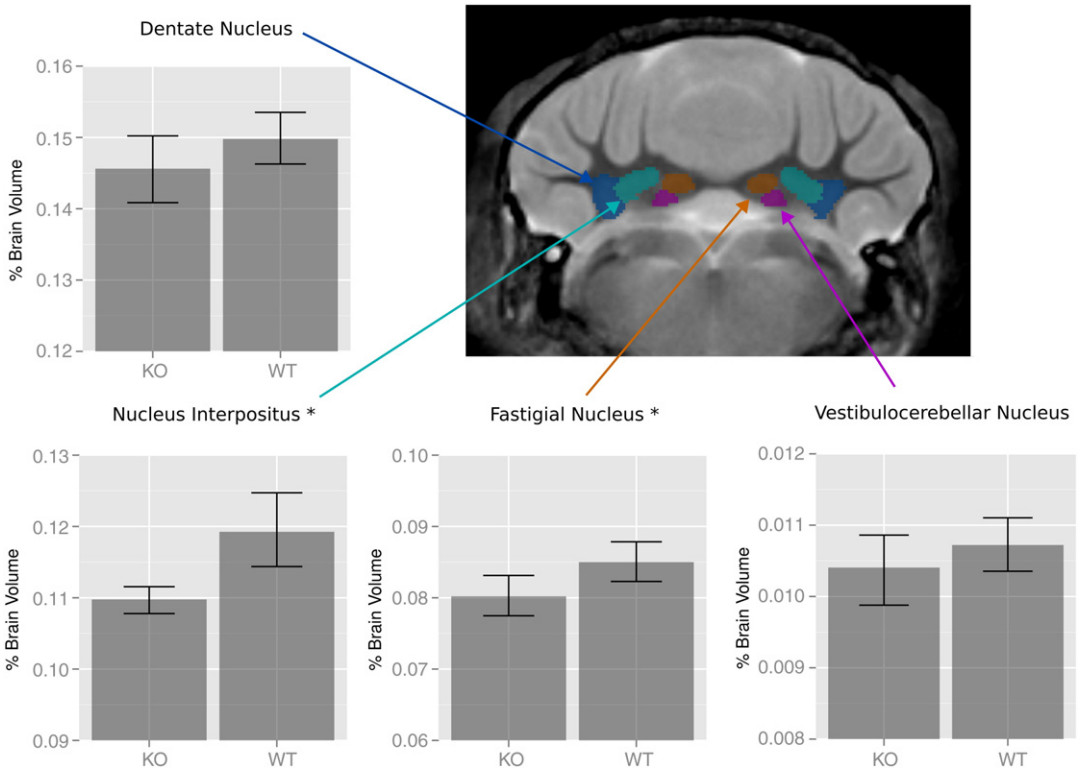

Fig. 3. Bar graphs representing the % total brain volume of the four cerebellar nuclei (nuclei volume is the summation of corresponding left and right nuclei). Error bars represent the 95% confidence interval. The volumes of the nucleus interpositus and the fastigial nucleus were found to be significantly different (*), with *p*-values of 0.002 and 0.038 respectively, when comparing the fragile X knockout mouse (KO) and the wild type (WT).

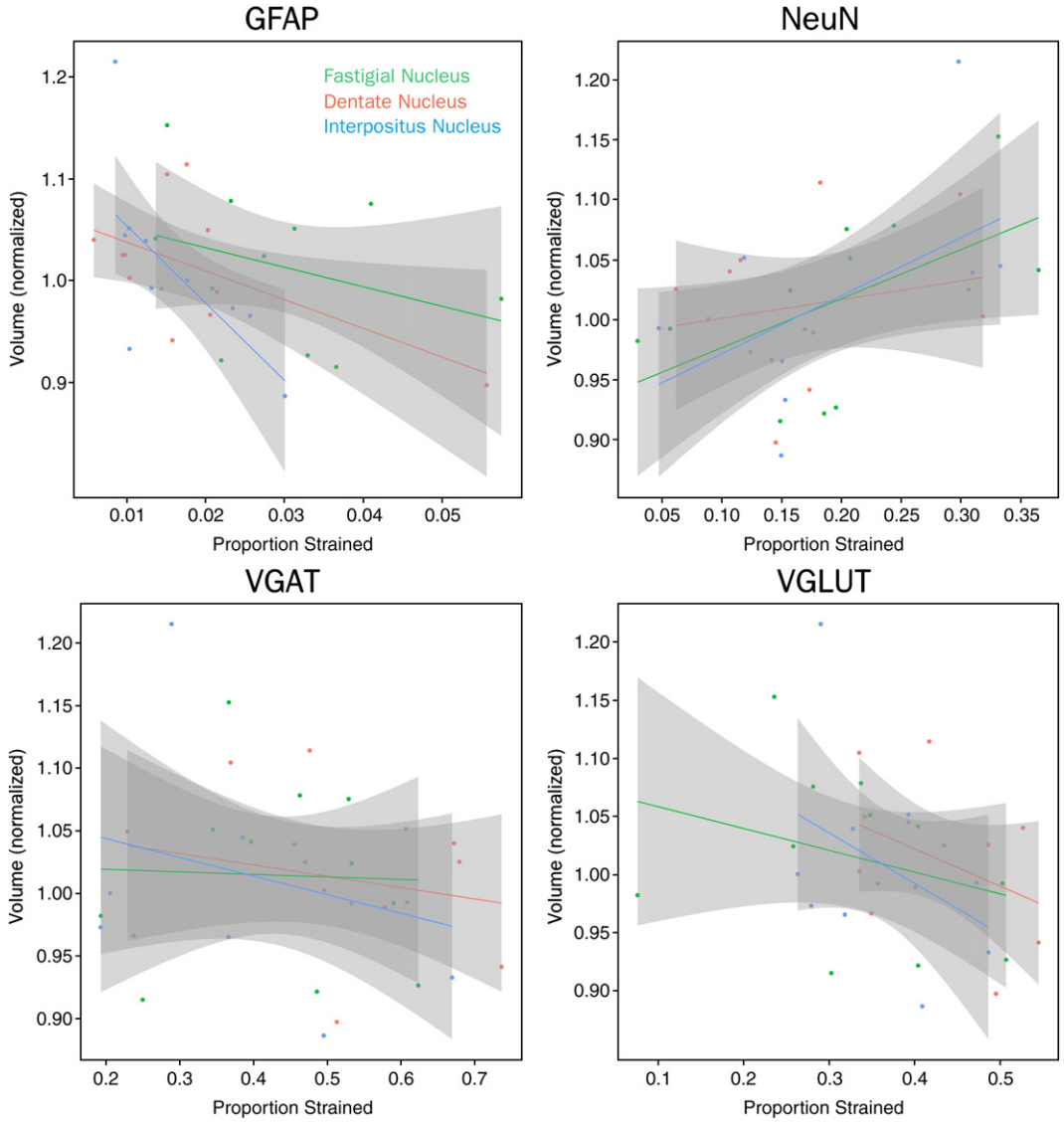

Fig. 4. Scatter plots showing the proportion of active stain in the 3 specific deep cerebellar nuclei, namely the fastigial nucleus, the dentate nucleus, and the nucleus interpositus, versus the normalized volume of those same 3 nuclei for each of the 4 stains used. Glial Fibrillary Acidic Protein (GFAP); Neuronal Nuclei (NeuN); Vesicular GABA Transporter (VGAT); Vesicular Glutamate Transporter 1 (VGLUT).

the cerebellar vermis (Courchesne et al., 1988; Reiss et al., 1988), which has been found to be underdeveloped and decreased in size in both disorders. The cerebellar vermis has known connections with the amygdala and hippocampus (Sacchetti et al., 2005) as well as the fastigial nucleus (Yamada and Noda, 1987). Therefore, the decrease in size in the fastigial nucleus seen here in the FX KO mouse could be correlated with changes seen in the cerebellar vermis in the human work.

The decrease in the striatal volume and the increase in the cerebral cortex of the parieto-temporal lobe found in the FX KO mouse are also interesting findings. Recent studies in 84 children and adolescents with FXS have revealed an increase in size of the caudate nucleus, as well as a decreased in the size of the cerebellar vermis, amygdala, and superior temporal gyrus (Gothelf et al., 2008). This increase in the caudate nucleus in human FXS; however, is in contrast to what was found here with a decrease in the striatum for FX KO mice. Furthermore, Stanfield et al. determined that the cerebral hemispheres increase in autism by analyzing several previous studies in a meta-analysis (Stanfield et al., 2008), which might also be related to the changes found in the cerebral cortex of the parieto-temporal lobe found in the FX KO model in this study. Volume differences in the FX KO mouse were originally examined in 1999 (Kooy et al., 1999), where the volume of 3 structures were reported (total brain volume, cerebellum, and 4th ventricle), as well as the surface area of mid-sagittal slices of the total brain, cerebellum (anterior and posterior), 4th ventricle, subcortical gray matter, and the hippocampus. In the Kooy study the cerebellum volume in the FX KO mouse, while found to be smaller ($70 \pm 3\ mm^3$) than the WT ($74 \pm 7\ mm^3$), was not significant. Further, the authors found no significant differences in any of the structures examined. The resolved voxel in the Kooy study was quite large ($4.2 \times 10^{-3}\ mm^3$) compared with this current work ($3.3 \times 10^{-5}\ mm^3$), probably accounting for the lack of any significance in that study.

With the changes in the arbor vita of the cerebellum and the changes in the deep cerebellar nuclei, the expectation was that changes in the white matter tracts would be visible with DTI. The DTI results, however, did not show any changes in the white matter structure between the FX KO and WT mouse in either a voxel by voxel comparison or in the mean FA values of the 62 different anatomical structures. FA values between WT and FX KO were very similar in all white matter regions, for example: corpus callosum—WT, $FA = 0.42 \pm 0.01$ (mean ± standard deviation) and FX KO, $FA = 0.42 \pm 0.02$; fimbria—WT, $FA = 0.52 \pm 0.01$

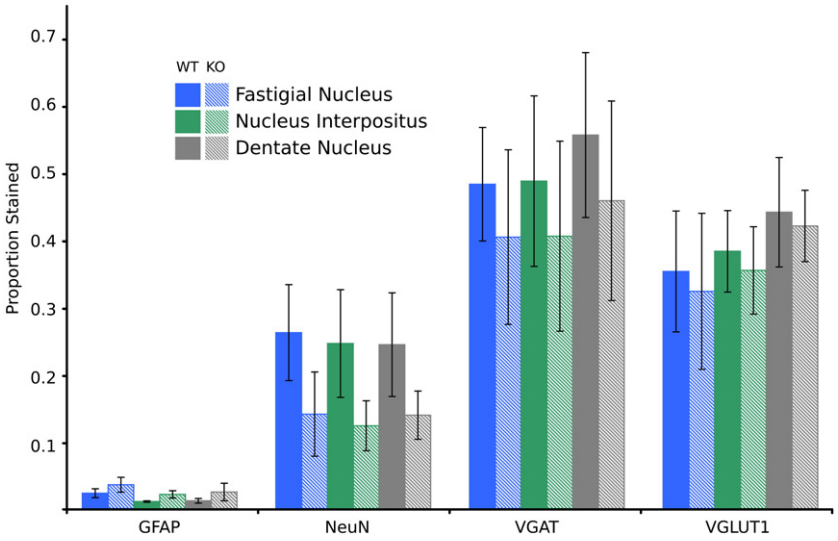

Fig. 5. Shows the proportion stained for the wild type (WT) and fragile X knockout (KO) in each 3 cerebellar nuclei examined for each of the four stains used. Error bars represent a 95% confidence interval. Glial Fibrillary Acidic Protein (GFAP); Neuronal Nuclei (NeuN); Vesicular GABA Transporter (VGAT); Vesicular Glutamate Transporter 1 (VGLUT).

and FX KO, FA = 0.52 ± 0.04; anterior commisure—WT, FA = 0.47 ± 0.02 and FX KO, FA = 0.45 ± 0.03. Previously, FA changes have been found in human fragile X patients in the fronto-striatal and parietal sensory motor pathways (Barnea-Goraly et al., 2003; Haas et al., 2009). The frontal striatal pathway changes may be related to the decrease seen in the volume of the striatum in the FX KO mouse; however, no changes were seen with the white matter structure in that area with current DTI measures. Fig. 6A depicts an average FA Map for the 7 WT mice, Fig. 6B is the average FA map for the 7 KO mice, clearly there are no noticeable differences. In order to determine the resolvable FA difference for a given voxel and region in the current data set, a specific voxel in the corpus callosum as well as the entire corpus callosum (as an example) were plotted to a power value of 0.8 against increasing group size (Fig. 6C). For a single voxel in the corpus callosum any significant difference would become evident at an FA difference of ± 0.05, for the entire structure of the corpus callosum significant differences would be resolved at an FA difference of ± 0.03 with 7 mice in each group. It is likely, therefore, that if there are FA differences between the FX KO and WT, they are very subtle. Some of the other known phenotypes of FX KO mice, such as the learning deficits, are also subtle and are often dependent on the background strain of the mice (Dobkin et al., 2000; Paradee et al., 1999).

We hypothesized that, with the long narrow face which is a hallmark of FXS, there may be some structural changes in the skull of the FX KO mouse. However, no changes were seen when compared to the WT. An example CT image from a single WT mouse used in this study can be seen in Fig. 7. Craniofacial abnormalities have been found in zebrafish (Tucker et al., 2006), which are attributed to dysmorphic cartilage formation. The Meckel's cartilage in the FXS zerbrafish embryo was found to be both shorter and wider when compared to the normal embryo (Tucker et al., 2006). No skeletal abnormalities have been found previously in mouse models of FXS. The lack of any significant finding may be due to the sensitivity of the method; however, again it is more likely due to the subtle nature of the mouse model used, since our method has been able to detect craniofacial changes in a mutant mice on the order of ~0.1 mm (Nieman et al., 2006).

Conclusions

Through the use of MRI imaging and immunohistochemical analysis, we have demonstrated anatomical changes the brains of FMR1 knockout mice (FX KO). These changes correlate with similar changes in human FXS, indicating that the methodology used in this study is useful for anatomical phenotyping in mouse models. Of

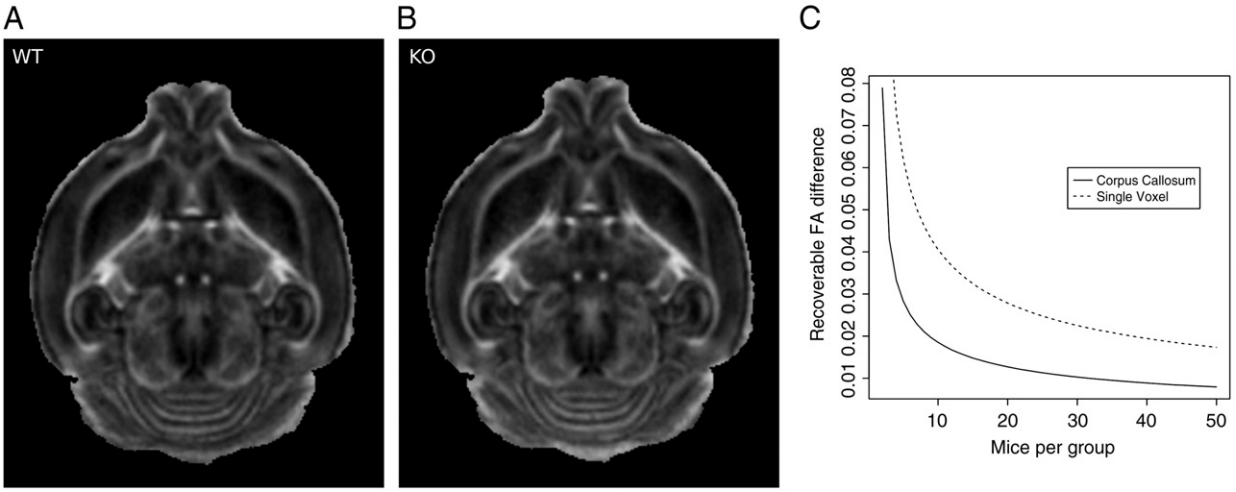

Fig. 6. Average Fractional Anisotropy (FA) maps of the wild type (A) and Fragile X knockout mouse (B). (C) The resolvable FA difference of a given voxel and the entire corpus callosum (as an example) to a power value of 0.8 plotted against the number of mice in each group.

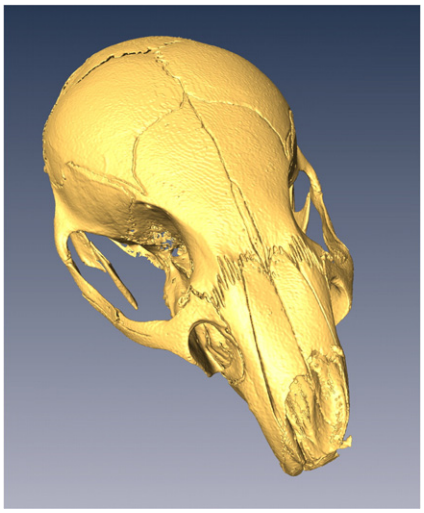

Fig. 7. 3D rendering of a single wild type mouse taken from our CT data set.

particular interest is the decreased volume of two deep cerebellar nuclei—the nucleus interpositus and the fastigial nucleus—in FX KO mice. Histological analyses of these nuclei suggest neuronal loss might account for the reduced volumes of these regions. However, further studies are needed to examine the effects of the loss of FMRP on the deep cerebellar nuclei and changes in this region might contribute to the pathogenesis of Fragile X syndrome.

References

Barnea-Goraly, N., Eliez, S., Hedeus, M., Menon, V., White, C.D., Moseley, M., Reiss, A.L., 2003. White matter tract alterations in fragile X syndrome: preliminary evidence from diffusion tensor imaging. Am. J. Med. Genet. B Neuropsychiatr. Genet. 118B, 81–88.

Bock, N.A., Nieman, B.J., Bishop, J.B., Mark Henkelman, R., 2005. In vivo multiple-mouse MRI at 7 Tesla. Magn. Reson. Med. 54, 1311–1316.

Collins, D.L., Neelin, P., Peters, T.M., Evans, A.C., 1994. Automatic 3D intersubject registration of MR volumetric data in standardized Talairach space. J. Comput. Assist. Tomogr. 18, 192–205.

Courchesne, E., Yeung-Courchesne, R., Press, G.A., Hesselink, J.R., Jernigan, T.L., 1988. Hypoplasia of cerebellar vermal lobules VI and VII in autism. N. Engl. J. Med. 318, 1349–1354.

Crawford, D.C., Acuna, J.M., Sherman, S.L., 2001. FMR1 and the fragile X syndrome: human genome epidemiology review. Genet. Med. 3, 359–371.

Curia, G., Papouin, T., Seguela, P., Avoli, M., 2009. Downregulation of tonic GABAergic inhibition in a mouse model of fragile X syndrome. Cereb. Cortex 19, 1515–1520.

Dobkin, C., Rabe, A., Dumas, R., El Idrissi, A., Haubenstock, H., Brown, W.T., 2000. Fmr1 knockout mouse has a distinctive strain-specific learning impairment. Neuroscience 100, 423–429.

Dorr, A.E., Lerch, J.P., Spring, S., Kabani, N., Henkelman, R.M., 2008. High resolution three-dimensional brain atlas using an average magnetic resonance image of 40 adult C57Bl/6J mice. Neuroimage 42, 60–69.

Dutch-Belgium Fragile X Consortium, 1994. Fmr1 knockout mice: a model to study fragile X mental retardation. The Dutch-Belgian Fragile X Consortium. Cell 78, 23–33.

Freeman Jr., J.H., Nicholson, D.A., 2000. Developmental changes in eye-blink conditioning and neuronal activity in the cerebellar interpositus nucleus. J. Neurosci. 20, 813–819.

Genovese, C.R., Lazar, N.A., Nichols, T., 2002. Thresholding of statistical maps in functional neuroimaging using the false discovery rate. Neuroimage 15, 870–878.

Gothelf, D., Furfaro, J.A., Hoeft, F., Eckert, M.A., Hall, S.S., O'Hara, R., Erba, H.W., Ringel, J., Hayashi, K.M., Patnaik, S., Golianu, B., Kraemer, H.C., Thompson, P.M., Piven, J., Reiss, A.L., 2008. Neuroanatomy of fragile X syndrome is associated with aberrant behavior and the fragile X mental retardation protein (FMRP). Ann. Neurol. 63, 40–51.

Grossman, A.W., Elisseou, N.M., McKinney, B.C., Greenough, W.T., 2006. Hippocampal pyramidal cells in adult Fmr1 knockout mice exhibit an immature-appearing profile of dendritic spines. Brain Res. 1084, 158–164.

Gruss, M., Braun, K., 2001. Alterations of amino acids and monoamine metabolism in male Fmr1 knockout mice: a putative animal model of the human fragile X mental retardation syndrome. Neural Plast. 8, 285–298.

Gruss, M., Braun, K., 2004. Age- and region-specific imbalances of basal amino acids and monoamine metabolism in limbic regions of female Fmr1 knock-out mice. Neurochem. Int. 45, 81–88.

Haas, B.W., Barnea-Goraly, N., Lightbody, A.A., Patnaik, S.S., Hoeft, F., Hazlett, H., Piven, J., Reiss, A.L., 2009. Early white-matter abnormalities of the ventral frontostriatal pathway in fragile X syndrome. Dev. Med. Child Neurol. 51, 593–599.

Henkelman, R.M., Baghdadi, L., Sled, J.G., 2006. Presentation of 3D isotropic imaging data for optimal viewing. Magn. Reson. Med. 56, 1371–1374.

Hessl, D., Rivera, S.M., Reiss, A.L., 2004. The neuroanatomy and neuroendocrinology of fragile X syndrome. Ment. Retard. Dev. Disabil. Res. Rev. 10, 17–24.

Irwin, S.A., Galvez, R., Greenough, W.T., 2000. Dendritic spine structural anomalies in fragile-X mental retardation syndrome. Cereb. Cortex 10, 1038–1044.

Jacobs, S., Doering, L.C., 2009. Astrocytes correct abnormal neuronal development in the Fragile X mouse model. Neuroscience Chicago.

Koekkoek, S.K., Yamaguchi, K., Milojkovic, B.A., Dortland, B.R., Ruigrok, T.J., Maex, R., De Graaf, W., Smit, A.E., VanderWerf, F., Bakker, C.E., Willemsen, R., Ikeda, T., Kakizawa, S., Onodera, K., Nelson, D.L., Mientjes, E., Joosten, M., De Schutter, E., Oostra, B.A., Ito, M., De Zeeuw, C.I., 2005. Deletion of FMR1 in Purkinje cells enhances parallel fiber LTD, enlarges spines, and attenuates cerebellar eyelid conditioning in Fragile X syndrome. Neuron 47, 339–352.

Kooy, R.F., Reyniers, E., Verhoye, M., Sijbers, J., Bakker, C.E., Oostra, B.A., Willems, P.J., Van Der Linden, A., 1999. Neuroanatomy of the fragile X knockout mouse brain studied using in vivo high resolution magnetic resonance imaging. Eur. J. Hum. Genet. 7, 526–532.

Le Bihan, D., Mangin, J.F., Poupon, C., Clark, C.A., Pappata, S., Molko, N., Chabriat, H., 2001. Diffusion tensor imaging: concepts and applications. J. Magn. Reson. Imaging 13, 534–546.

Lerch, J.P., Carroll, J.B., Spring, S., Bertram, L.N., Schwab, C., Hayden, M.R., Henkelman, R.M., 2008. Automated deformation analysis in the YAC128 Huntington disease mouse model. Neuroimage 39, 32–39.

Mostofsky, S.H., Mazzocco, M.M., Aakalu, G., Warsofsky, I.S., Denckla, M.B., Reiss, A.L., 1998. Decreased cerebellar posterior vermis size in fragile X syndrome: correlation with neurocognitive performance. Neurology 50, 121–130.

Musumeci, S.A., Bosco, P., Calabrese, G., Bakker, C., De Sarro, G.B., Elia, M., Ferri, R., Oostra, B.A., 2000. Audiogenic seizures susceptibility in transgenic mice with fragile X syndrome. Epilepsia 41, 19–23.

Nieman, B.J., Flenniken, A.M., Adamson, S.L., Henkelman, R.M., Sled, J.G., 2006. Anatomical phenotyping in the brain and skull of a mutant mouse by magnetic resonance imaging and computed tomography. Physiol. Genomics 24, 154–162.

Nimchinsky, E.A., Oberlander, A.M., Svoboda, K., 2001. Abnormal development of dendritic spines in FMR1 knock-out mice. J. Neurosci. 21, 5139–5146.

O'Donnell, W.T., Warren, S.T., 2002. A decade of molecular studies of fragile X syndrome. Annu. Rev. Neurosci. 25, 315–338.

Oostra, B.A., Hoogeveen, A.T., 1997. Animal model for fragile X syndrome. Ann. Med. 29, 563–567.

Pacey, L.K., Doering, L.C., 2007. Developmental expression of FMRP in the astrocyte lineage: implications for fragile X syndrome. Glia 55, 1601–1609.

Pacey, L.K., Heximer, S.P., Hampson, D.R., 2009. Increased GABA(B) receptor-mediated signaling reduces the susceptibility of fragile X knockout mice to audiogenic seizures. Mol. Pharmacol. 76, 18–24.

Paradee, W., Melikian, H.E., Rasmussen, D.L., Kenneson, A., Conn, P.J., Warren, S.T., 1999. Fragile X mouse: strain effects of knockout phenotype and evidence suggesting deficient amygdala function. Neuroscience 94, 185–192.

Reiss, A.L., Patel, S., Kumar, A.J., Freund, L., 1988. Preliminary communication: neuroanatomical variations of the posterior fossa in men with the fragile X (Martin–Bell) syndrome. Am. J. Med. Genet. 31, 407–414.

Reiss, A.L., Freund, L., Tseng, J.E., Joshi, P.K., 1991. Neuroanatomy in fragile X females: the posterior fossa. Am. J. Hum. Genet. 49, 279–288.

Reiss, A.L., Lee, J., Freund, L., 1994. Neuroanatomy of fragile X syndrome: the temporal lobe. Neurology 44, 1317–1324.

Reiss, A.L., Abrams, M.T., Greenlaw, R., Freund, L., Denckla, M.B., 1995. Neurodevelopmental effects of the FMR-1 full mutation in humans. Nat. Med. 1, 159–167.

Sacchetti, B., Scelfo, B., Strata, P., 2005. The cerebellum: synaptic changes and fear conditioning. Neuroscientist 11, 217–227.

Spring, S., Lerch, J.P., Henkelman, R.M., 2007. Sexual dimorphism revealed in the structure of the mouse brain using three-dimensional magnetic resonance imaging. Neuroimage 35, 1424–1433.

Stanfield, A.C., McIntosh, A.M., Spencer, M.D., Philip, R., Gaur, S., Lawrie, S.M., 2008. Towards a neuroanatomy of autism: a systematic review and meta-analysis of structural magnetic resonance imaging studies. Eur. Psychiatry 23, 289–299.

Tabuchi, K., Blundell, J., Etherton, M.R., Hammer, R.E., Liu, X., Powell, C.M., Sudhof, T.C., 2007. A neuroligin-3 mutation implicated in autism increases inhibitory synaptic transmission in mice. Science 318, 71–76.

Thompson, R.F., Steinmetz, J.E., 2009. The role of the cerebellum in classical conditioning of discrete behavioral responses. Neuroscience 162, 732–755.

Tucker, B., Richards, R.I., Lardelli, M., 2006. Contribution of mGluR and Fmr1 functional pathways to neurite morphogenesis, craniofacial development and fragile X syndrome. Hum. Mol. Genet. 15, 3446–3458.

Visootsak, J., Warren, S.T., Anido, A., Graham Jr., J.M., 2005. Fragile X syndrome: an update and review for the primary pediatrician. Clin. Pediatr. (Phila) 44, 371–381.

Yamada, J., Noda, H., 1987. Afferent and efferent connections of the oculomotor cerebellar vermis in the macaque monkey. J. Comp. Neurol. 265, 224–241.

Zijdenbos, A.P., Forghani, R., Evans, A.C., 2002. Automatic "pipeline" analysis of 3-D MRI data for clinical trials: application to multiple sclerosis. IEEE Trans. Med. Imaging 21, 1280–1291.